Stable Dropwise Condensation for Enhancing Heat Transfer via the Initiated Chemical Vapor Deposition (iCVD) of Grafted Polymer Films

Stable Dropwise Condensation for Enhancing Heat Transfer via the Initiated Chemical Vapor Deposition (iCVD) of Grafted Polymer Films

Adam T. Paxson, Jose L. Yagüe, Karen K. Gleason, Kripa K. Varanasi**

Adam T. Paxson, Prof. Kripa K. Varanasi
Department of Mechanical Engineering, 77 Massachusetts Avenue, Cambridge, MA, 02139, United States
E-mail: varanasi@mit.edu
Dr. Jose L. Yagüe, Prof. Karen K. Gleason,
Department of Chemical Engineering, 77 Massachusetts Avenue, Cambridge, MA, 02139, United States

Keywords: surface functionalization, chemical vapor deposition, crosslinking, fluoropolymers, wettability

Condensation of water vapor is a crucial process in many industries, including power generation and desalination. Roughly 85% of the global installed base of electricity generation plants and 50% of desalination plants worldwide rely on steam condensers.[1][2] Given the massive scale of these processes, any improvements in cycle efficiencies would have a profound effect on global energy consumption. Dropwise condensation has been an active area of research for nearly a century, as the resulting heat transfer coefficients can be an order of magnitude higher than those seen in filmwise condensation.[3][4] However, the practical implementation of this concept in power generation, desalination, and other applications has been a significant materials challenge,[4] limited by durability of existing hydrophobic functionalization for metal heat transfer surfaces. While metals provide both high thermal conductivity for maximizing heat transfer and high tensile strength to minimize the need for structural supports, metals are typically wetted by water and most other thermal fluids and so exhibit filmwise condensation. Thus, metallic heat transfer surfaces must be modified with a hydrophobic coating to obtain dropwise condensation. Previous dropwise promoters have included self-assembled monolayers of oleic acids,[5][6] fatty acids, and also of thin films of polymers applied via sputtering or dip-coating.[7]–[9] However, most of these hydrophobic modifiers, and especially the silane-based modifiers that are ubiquitous in recent

condensation studies, are not robust in steam environments of industrial interest. More recent studies have used nanotextured surfaces to improve condensation heat transfer, however these surfaces also rely on silane or thiol modifiers to switch the wettability of a nanotextured surface from superhydrophilic to superhydrophobic.[10]–[19] Additionally, because the thermal conductivities of polymeric materials are typically orders of magnitude smaller than that of a metal substrate, it is crucial that a polymer modifier be as thin as possible to minimize thermal resistance. Hence, there is a need for an ultra-thin robust hydrophobic modifier.

In this communication, we report the sustained dropwise condensation of steam on a thin film of poly-(1H,1H,2H,2H-perfluorodecyl acrylate)-*co*-divinyl benzene p(PFDA-*co*-DVB) grafted to a metal substrate by initiated chemical vapor deposition (iCVD). The heat transfer performance and durability of this coating are compared to a coating of trichloro(1*H*,1*H*,2*H*,2*H*-perfluorooctyl)silane (fluorosilane).

The iCVD process is a single-step, solvent-free, low-energy, vapor-phase method used to deposit conformal films with precisely controllable thickness and in which grafting to the substrate provides enhanced durability. [20] The large choice of monomers allows for the design of surface properties. For the current application, a combination of durability and low contact angle hysteresis is desired. Copolymerization with a crosslinker is an additional means to render the films more stable to chemical and mechanical degradation. While liquid-based solution approaches to copolymer synthesis commonly require that the two monomers have a common solvent, the use of vapor synthesis removes this constraint. It has been recently demonstrated that iCVD allows the non-fluorinated crosslinker, DVB, to be readily copolymerized with the fluorinated monomer, PFDA, over its entire compositional range.[21] Copolymerization also disrupts crystallization. Since crystallites are one source of roughness, copolymer films are anticipated to be smoother than crystalline iCVD p(PFDA) homopolymer

layers. Additionally, the perfluorinated side chains of the PFDA units segregate to the interface under dry conditions in order to minimize surface energy. Surface reconstruction in which the perfluoro chains orient away from the interface can occur when the surface becomes wet.[22]

Briefly, monomer and initiator species (**Figure 1a**) are flowed into a reactor at controlled rates and encounter heated filaments and a cooled substrate (Figure 1b). The locally heated zone around the filaments thermally cleaves the initiator species (tert-butyl peroxide, TBPO). The radical fragments produced initiate vinyl polymerization of the monomers absorbed on the surface, which is held at a lower temperature. The functional groups, such as the perfluorinated side chain of PFDA, are fully preserved after polymerization.[23] The iCVD of the homopolymers p(PFDA) and p(DVB) results in highly conformal thin films, [23]–[25] and superhydrophobic and superoleophobic surfaces have been demonstrated with iCVD films of p(PFDA). Recently, iCVD copolymer films of p(PFDA-*co*-DVB) were integrated into photonic circuits as an athermal cladding.[26] This approach also allows for ultra-thin films, which are needed to minimize the total thermal resistance from the condensing vapor to the coolant. The total thermal resistance includes the following resistances in series: the resistance from the condensing vapor to the substrate, the conduction resistance through the film and the substrate, and the convection resistance of the coolant: $R_T = R_s + R_f + R_m + R_w = \left(\frac{1}{h_s}\right) + \left(\frac{l}{k}\right)_f + \left(\frac{l}{k}\right)_m + \left(\frac{1}{h_w}\right)$ (1)

where the subscripts *s*, *f*, *m*, and *w* represent the steam condensation, film conduction, metal conduction, and water convection, respectively. Typical orders of magnitude of the variables are as follows: [27] $h_s \approx 10^4$ W·m^{-2}·K^{-1}, $k_f \approx 10^{-1}$ W·m^{-1}·K^{-1}, $l_f \approx 10^{-3}$ m, $k_m \approx 10^2$ W·m^{-1}·K^{-}1, $h_w \approx 10^3$ W·m^{-2}·K^{-1}. Thus, the total resistance of the condenser is of the order 10^{-3} K·m·W^{-1}, whereas the conduction resistance due to the film is of the order 10^{-8} K·m·W^{-1}. To optimize

the film thickness and ensure that the conduction resistance of the polymer film contributes no more than 1% of the total resistance, the thickness must be less than 1 μm. Since the present coating is so thin, it represents only 0.5% of the condensation resistance and ~0.001% of the total thermal resistance. This is in contrast to the polymer films in previous studies that were many microns thick.[28]–[31]

The film thickness is measured *in-situ* during deposition, so that the process can be stopped when the thickness reaches the desired value. In all cases, the iCVD copolymer layers were ultra-thin (~40 nm), leading to an estimated contribution to total thermal resistance of less than 0.001%. To verify that the film thickness did not have an effect on the condensation heat transfer coefficient, we measured two different thicknesses of films and provide a summary of the results in Table 1. We find the condensation heat transfer coefficients of the two film thicknesses to be nearly identical.

The dropwise heat transfer coefficient is strongly influenced by the size of the departing drops.[4][32] Since a condensate drop begins to present a thermal resistance as soon as it forms, it is desirable to shed condensate drops as quickly as possible. External forces such as gravity or vapor shear may be utilized to remove condensate droplets, but they need to overcome the pinning forces due to surface tension that anchor the contact line of the drop to the condensing surface.[33][34] A lower contact angle hysteresis (CAH) will result in shedding of condensate drops at a smaller size, and thus a larger heat transfer coefficient. Previous work on p(PFDA-*co*-DVB) homopolymer coatings have shown that the hysteresis can be significantly reduced by immobilizing the polymer chains via crystallization,[25] grafting to the substrate,[24] and crosslinking followed by thermal annealing.[21]

Figure 1c shows the high-resolution C1s x-ray photoelectron spectra (XPS) of the iCVD p(PFDA-*co*-DVB) copolymer surface. The pendant groups from the PFDA consist of –C*F_2-

and C*F_3 and these two bonding environments can be readily resolved at 290.8 and 293.1 eV, respectively. In aggregate, these fluorinated carbon groups account for 61.8 ± 0.4% of the area of the spectrum. The assignments at lower binding energies represent carbon atoms directly bonded only to oxygen, hydrogen, or other carbon atoms. However, the precise assignments of the peaks at lower binding energy is ambiguous due to the multitude of environments arising from the main acrylate portion of the PFDA and from the DVB.

The CF_2 and CF_3 bonding environments were previously observed in C1s XPS spectrum of the iCVD PFDA homopolymer,[23] representing a combined area of 61.4 ± 0.3%, in agreement with the structural formula for PFDA which gives a theoretical value of 61.5%. The similarity with homopolymer results suggests the degree of DVB crosslinker incorporation in the copolymer in the near surface region probed by XPS is quite low. Thus, the surface properties of the copolymer in the dry state, such as the advancing contact angle, will be dominated by the PFDA units. When examined by Fourier transform infrared spectra (FTIR), which penetrates the entire film thickness, sp^2 C-H stretching modes between 2810 and 2890 cm^{-1} are observed, confirming the incorporation of the DVB in the bulk of the film.[21][26] These underlying crosslinking units are anticipated to reduce the ability of the surface layer to reconstruct between the dry and wet states, potentially reducing this contribution to contact angle hysteresis. By following a deposition of PFDA:DVB 0.2:0.6 sccm with a thermal annealing step, the advancing and receding water contact angles on the resultant thin film are 132 ± 1° and 127° ± 1.2°, respectively, with a CAH of 5°. Average film thicknesses were measured by ellipsometry,[35] AFM, and contact profilometry to be 41.5 ± 2.4 nm. AFM scans (Figure 1d, e) show that the surface is covered by structures with a height of ~100 nm and an average spacing of 1.3 ± 0.7 μm, resulting in an RMS roughness of 75 nm. These rough features are semicrystalline aggregates formed at nucleation sites during the condensation polymerization reaction of the monomers. Previous literature has shown that $–(CF_2)_nCF_3$

chains with $n \geq 7$ leads to aggregates in a smectic B structure that arrange into a rotationally symmetric fiber texture.[25][36] On the other hand, the fluorosilane surface, which is composed of larger, less sterically-hindered functional groups[37] with a thickness of 2.5 nm and an RMS roughness of 1.5 ± 0.3 nm, exhibited a CAH of 25° ± 3°. Since the roughness of the silanized surface is lower than that of the copolymer surface, morphology alone cannot explain the lower hysteresis of the copolymer surface. Instead, we attribute this to the steric hindrance induced by the crosslinking that prevents the CF_3 groups from shifting away from their low-energy unwetted state.

In addition to contact angle hysteresis, the dropwise condensation heat transfer coefficient depends on a number of complex factors including nucleation site density and population distribution.[32][38]–[40] To investigate the behavior of these surfaces during condensation, we condensed saturated pure water vapor at 800 Pa while cooling the surface with a Peltier device to a supersaturation of 1.16 ± 0.05 and imaging with an environmental scanning electron microscope (ESEM). During the pre-coalescence growth regime,[41] we note that the nucleation density on the copolymer surface (173 ± 19 mm^{-2}, **Figure 2a**) is significantly higher than that on a fluorosilane surface (110 ± 10 mm^{-2}, Figure 2b) most likely owing to the rougher surface providing a larger number of concavities that act as nucleation sites.[42] During condensation of an air stream saturated with water vapor under ambient conditions (21°C, 40% RH), the departing diameter is 2.0 ± 0.3 mm (Figure 2c). This is considerably smaller than the departing drop sizes on other common hydrophobic modifiers such as gold (3.3 mm) and oleic acid (4.3 mm)[43]. When compared to a silanized silicon surface with a departing diameter of 2.9 ± 0.2 mm (Figure 2d), we also observe a shift in the distribution of droplet diameters to smaller sizes (Figure 2e). The increased nucleation density, lower departure diameter, and droplet size distribution of the copolymer surface on a smooth silicon

substrate all suggest an improved condensation heat transfer coefficient according to widely-accepted models.

Commercial condensers are typically constructed using alloys of metals such as titanium, stainless steel, copper, and aluminum. To move towards an industrially relevant prototype, we grafted a 40 nm film of p(PFDA-*co*-DVB) onto 50 mm diameter aluminum substrates. The additional roughness imparted by the metal surface (RMS = 118 ± 33 nm) is apparent in the AFM height scans (**Figure 3 a, b**). As expected on a rougher surface wetting in a Wenzel state, the CAH measured in air is notably higher (32° ± 2°). The CAH measured during condensation at 6.9 kPa is similar (37° ± 5°) and accordingly, the size of a departing drop (4.2 ± 0.1 mm) is larger than that on a silicon substrate (Figure 3c).

Accelerated endurance tests were conducted by condensing steam at 100°C. Coatings of p(PFDA-*co*-DVB) were compared to fluorosilane coatings, both on aluminum substrates (Figure 3c, d). Figure 3e shows a comparison of these two surfaces, along with an uncoated aluminum surface that undergoes filmwise condensation for reference, under prolonged condensation at 103.4 kPa. Although the silanized surface initially displays a larger heat transfer coefficient of 61 ± 2 kW m^{-2} K^{-1} due to the lower hysteresis (31° ± 3°) and departing droplet size (3.6 ± 0.4 mm), it quickly degrades in a matter of minutes and exhibits filmwise condensation with a heat transfer coefficient of 4.6 ± 0.4 kW m^{-2} K^{-1}. The grafted polymer coating exhibits dropwise condensation with a departing droplet size of 4.2 ± 0.1 mm and a heat transfer coefficient greater than 35 kW m^{-2} K^{-1}, which is more than 7 times greater than the steady-state filmwise heat transfer coefficient of the degraded silanized surface, with no noticeable degradation after 48 hours of condensation.

As a further demonstration of the versatility of iCVD-deposited copolymers to coat complex shapes such as heat exchanger tubing, we grafted a 40nm thin film of p(PFDA-*co*-DVB) conformally onto the outer surface of a copper tubing coil. It would be difficult to achieve such an ultra-thin, uniform layer by common surface modification techniques such as spray coating, spin casting and doctor blade application, or with vacuum techniques such as sputtering and evaporation. As seen in **Figure 4**, the tubing coil exhibited dropwise condensation after a single-step deposition.

In conclusion, we demonstrate that grafted polymers deposited via iCVD lead to robust dropwise condensing surfaces that can sustain prolonged exposure (> 48 hours) to steam at 100°C, significantly outperforming a fluorosilane treatment tested under identical conditions. The unique composition of the copolymer achievable by iCVD is essential for achieving low contact angle hysteresis, which results from the combination of low roughness and limited reorientation of the surface fluorinated groups between the wet and dry states. iCVD surfaces exhibit heat transfer coefficients that are more than 7 times greater than filmwise condensation when deposited on practical engineering heat transfer substrates, such as aluminum and copper. A successful prototype has been demonstrated with a modified heat exchanger tube, demonstrating the potential for scale-up to industrial processes.

Experimental Section

iCVD coatings: iCVD polymerizations were conducted in a custom-design cylindrical reactor (diameter 24.6 cm and height 3.8 cm), supporting an array of 14 parallel chromoalloy filaments (Goodfellow) suspended 2 cm from the stage. Tert-butyl peroxide (TBPO) (98%, Aldrich), PFDA (97%, Aldrich) and DVB (80%, Aldrich) were used as received. The peroxide initiator, TBPO, was delivered into the reactor through a mass flow controller (MKS Instruments) at a constant flow rate of 3.2 sccm. PFDA and DVB were vaporized in glass jars

that were heated to 80 and 60ºC respectively. The flow rates were controlled using needle valves and kept constant at 0.2 and 0.6 sccm. The filaments were resistively heated to 230ºC using a DC power supply (Sorensen), and the temperature was measured by a K-type thermocouple (Omega Engineering). The sample stage was backcooled at 30ºC using a recirculating chiller/heater (Neslab RTE-7). The working pressure was maintained at 200 mTorr using a throttle valve (MKS Instruments). The reactor was covered with a quartz top (2.5 cm) that allows in-situ thickness monitoring by interferometry with a 633 nm HeNe laser source (JDS Uniphase). Final thickness of the copolymer deposited on the metal substrate corresponds to 40 nm. Afterwards, a thermal annealing process was performed by introducing the sample in an oven (VWR) at 80ºC for 30 min. The full width at half-maximum (FWHM) was fixed at 2-3 eV to take into account the broadening of the 1 eV electron beam, while using XPS Scienta Database F1s peaks with FWHM of 2 eV.

Silanization: To deposit silane coatings, substrates were first cleaned by sonication in acetone for 5 minutes, followed by rinsing in DI water (18 MOhm), followed by sonication in isopropanol for 5 minutes, and finally a rinse with DI water. The surfaces were treated with oxygen plasma for 10 minutes for further cleaning and for creating surface hydroxyl groups. After plasma treatment, the surfaces were immediately placed in a vacuum desiccator along a small open vial containing 100 µL of either trichlorovinylsilane (97%, Sigma Aldrich) as a precursor for the polymer films or trichloro(1*H*,1*H*,2*H*,2*H*-perfluorooctyl)silane (97%, Sigma Aldrich) as the fluorosilane coating. The chamber was pumped down to 20 torr and the chamber was isolated to allow the silane to vaporize. The chamber was purged twice more, then isolated. The silane was allowed to vaporize and react with the substrate for 2 hours. After deposition, the surfaces were sonicated in toluene to remove excess unreacted silane and rinsed with DI water.

Film thickness measurement: Film thicknesses were measured with variable-angle ellipsometric spectroscopy (VASE, M-2000, J. A. Woollam) and by measuring scratch step height with atomic force microscopy (AFM, MP3D-SA, Asylum) and contact profilometry (Model 150, Dektak). All VASE thickness measurements were performed at a 70° incidence angle using 190 wavelengths from 315 to 718 nm. A nonlinear least-squares minimization was used to fit ellipsometric data of dry films to the Cauchy-Urbach model. The thickness was obtained upon convergence of the algorithm. FTIR measurements were performed on a Nicolet Nexus 870 ESP spectrometer in normal transmission mode equipped with a MCT (mercury cadmium tellurium detector and KBr beamsplitter. Spectra were acquired over the range of 400 to 4000 cm-1 with a 4 cm-1 resolution for 256 scans. All AFM thickness measurements were performed in tapping mode over an area of 20 μm x 20 μm using a cantilever with a tip radius of 9 ± 2 nm (AC200TS, Asylum). The film thickness was calculated as the difference between the average heights of the rough film surface and the trough of the scratch; the rough built-up edge of the scratch was masked from analysis. The profilometry measurements were performed with a stylus having a radius of 12.5 μm. The film thickness was similarly calculated as the difference in the average height of the rough film and the smooth scratch trough. AFM and profilometry measurements were repeated on at least four locations. Film thickness is reported as the mean and standard deviation of all measurements.

Surface roughness measurement: Surface roughness was measured using atomic force microscopy (AFM, MP3D-SA, Asylum) in tapping mode. The advancing and receding contact angles were measured using a goniometer (Model 590 Advanced, ramé-hart). The hysteresis was also measured during condensation on the grafted polymer sample as the difference between the receding and advancing ends of a drop immediately before departure.

Contact angles during condensation on the silanized sample could not be measured due to the film covering the surface.

ESEM condensation: 2 mm x 2 mm sample substrates were secured to an aluminum stub with double-sided carbon adhesive and instrumented with a K-type thermocouple embedded into the tape. The aluminum stub was clamped into a Peltier cooling stage (Coolstage Mk 2, Deben) which was attached to the stage of an environmental scanning electron microscope (EVO 55, Zeiss). The chamber was purged with water vapor three times up to 3 kPa and down to 10 Pa to remove non-condensable gases. After purging, the pressure was held at 800 Pa and the temperature was slowly decreased at a rate of 0.5 K min^{-1} until formation of observable water droplets (> 1 µm diameter). Accelerating voltage was 20 kV and beam current was 100 nA. Images were recorded at ~1Hz and the stage was moved to different areas to avoid charging effects on nucleation. Nucleation densities were measured as the mean and standard deviation of at least five different locations on each surface.

Steam condensation: Details of the condensation apparatus are described elsewhere.[44] Briefly, coated condensing specimens were secured in a chamber with the coated side exposed to saturated steam and the other side cooled by circulating water. The chamber was initially evacuated to below 100 mTorr to remove non-condensable vapors, and steam was introduced at a variable rate to maintain pressures ranging from 6.9 kPa to 103 kPa. Temperature gradients within the specimens were measured by thermistors embedded at precisely known locations within the sample. The heat transfer coefficient could be determined from the temperature gradient and the surface temperature. Saturated steam was produced by an electric boiler using deionized feedwater with a resistivity of 5 MOhm that was fed through a degassifier to reduce dissolved oxygen to below 1 ppm. The rear side of the sample was cooled by a forced chilled water at 4°C.

Acknowledgements
A.T.P. gratefully acknowledges funding support from the NSF GRFP and support from NSF Career award no. ECS-0335765. This research was performed in part at the Institute for Soldier Nanotechnologies (ISN) supported in part by the U.S. Army Research Office under contract W911NF-13-D-0001. This work made use of the Cornell Center for Materials Research Shared Facilities, which are supported through the NSF MRSEC program (DMR-1120296). This work was performed in part at the Center for Nanoscale Systems (CNS), a member of the National Nanotechnology Infrastructure Network (NNIN), which is supported by the National Science Foundation under NSF award no. ECS-0335765. CNS is part of Harvard University.

[1] *World Energy Outlook 2010*, International Energy Agency OECD Publications, Paris, France **2010**.
[2] *Human Development Report 2006*, United Nations Development Program Publications, New York, NY, USA **2006**.
[3] E. Schmidt, W. Schurig, W. Sellschopp, *Tech. Mech. Thermodyn.* **1930**, *1*, 53.
[4] J. Rose, *Proc. Inst. Mech. Eng. Part J. Power Energy* **2002**, *216*, 115.
[5] R.W. Bonner, in *Proc. Int. Heat Transf. Conf.*, Washington, DC, USA **2010**.
[6] R.A. Erb, *J. Phys. Chem.* **1965**, *69*, 1306.
[7] K.M. Holden, A.S. Wanniarachchi, P.J. Marto, D.H. Boone, J.W. Rose, *J. Heat Transf.* **1987**, *109*, 768.
[8] N. Yoshida, Y. Abe, H. Shigeta, A. Nakajima, H. Ohsaki, K. Hashimoto, T. Watanabe, *J. Am. Chem. Soc.* **2005**, *128*, 743.
[9] J.R. Lara, M.T. Holtzapple, *Desalination* **2011**, *280*, 363.
[10] K. Varanasi, M. Hsu, N. Bhate, W. Yang, T. Deng, *Appl. Phys. Lett.* **2009**, *95*, 094101.
[11] M. He, Q. Zhang, X. Zeng, D. Cui, J. Chen, H. Li, J. Wang, Y. Song, *Adv. Mater.* **2013**, *25*, 2291.
[12] X. Chen, J. Wu, R. Ma, M. Hua, N. Koratkar, S. Yao, Z. Wang, *Adv. Funct. Mater.* **2011**, *21*, 4617.
[13] J. Boreyko, C. Chen, *Phys. Rev. Lett.* **2009**, *103*, 184501.
[14] C. Dorrer, J. Rühe, *Adv. Mater.* **2008**, *20*, 159.
[15] S. Anand, A.T. Paxson, R. Dhiman, J.D. Smith, K.K. Varanasi, *ACS Nano* **2012**, *6*, 10122.
[16] N. Miljkovic, R. Enright, Y. Nam, K. Lopez, N. Dou, J. Sack, E.N. Wang, *Nano Lett.* **2012**, *13*, 179.
[17] K. Rykaczewski, A.T. Paxson, S. Anand, X. Chen, Z. Wang, K.K. Varanasi, *Langmuir* **2013**, *29*, 881.
[18] D.M. Anderson, M.K. Gupta, A.A. Voevodin, C.N. Hunter, S.A. Putnam, V.V. Tsukruk, A.G. Fedorov, *ACS Nano* **2012**, *6*, 3262.
[19] D. Torresin, M.K. Tiwari, D. Del Col, D. Poulikakos, *Langmuir* **2013**, *29*, 840.
[20] M.E. Alf, A. Asatekin, M.C. Barr, S.H. Baxamusa, H. Chelawat, G. Ozaydin-Ince, C.D. Petruczok, R. Sreenivasan, W.E. Tenhaeff, N.J. Trujillo, S. Vaddiraju, J. Xu, K.K. Gleason, *Adv. Mater.* **2010**, *22*, 1993.
[21] J.L. Yagüe, K.K. Gleason, *Macromolecules* **2013**.
[22] S.H. Baxamusa, K.K. Gleason, *Adv. Funct. Mater.* **2009**, *19*, 3489.
[23] M. Gupta, K.K. Gleason, *Langmuir* **2006**, *22*, 10047.
[24] A.M. Coclite, Y. Shi, K.K. Gleason, *Adv. Mater.* **2012**, *24*, 4534.
[25] A.M. Coclite, Y. Shi, K.K. Gleason, *Adv. Funct. Mater.* **2012**, *22*, 2167.

[26] V. Raghunathan, J.L. Yagüe, J. Xu, J. Michel, K.K. Gleason, L.C. Kimerling, *Opt. Express* **2012**, *20*, 20808.
[27] J.H. Lienhard, R. Eichhorn, J.H. Lienhard, *A Heat Transfer Textbook*, Prentice-Hall**1987**.
[28] S. Stylianou, J. Rose, *J. Heat Transf.* **1980**, *102*.
[29] R. Wilmshurst, J. Rose, **1970**.
[30] C. Graham, *The Limiting Heat Transfer Mechanisms of Dropwise Condensation.*, Ph.D Thesis, Massachusetts Institute of Technology, **1969**.
[31] K.P. Perkins, *An Experimental Study of Dropwise Condensation on Vertical Discs.*, **1979**.
[32] B.S. Sikarwar, S. Khandekar, S. Agrawal, S. Kumar, K. Muralidhar, *Heat Transf. Eng.* **2012**, *33*, 301.
[33] J.F. Joanny, P.G. de Gennes, *J. Chem. Phys.* **1984**, *81*, 552.
[34] D. Quere, *Reports Prog. Phys.* **2005**, *68*, 2495.
[35] K.K.S. Lau, J.A. Caulfield, K.K. Gleason, *J. Vac. Sci. Technol. Vac. Surfaces Films* **2000**, *18*, 2404.
[36] A. Takahara, N. Morotomi, S. Hiraoka, N. Higashi, T. Kunitake, T. Kajiyama, *Macromolecules* **1989**, *22*, 617.
[37] N. Belman, K. Jin, Y. Golan, J.N. Israelachvili, N.S. Pesika, *Langmuir* **2012**, *28*, 14609.
[38] J. Rose, *Int. Commun. Heat Mass Transf.* **1988**, *15*, 449.
[39] R.J. Hannemann, B.B. Mikic, *Int. J. Heat Mass Transf.* **1976**, *19*, 1299.
[40] V.P. Carey, *Liquid-Vapor Phase-Change Phenomena*, Taylor & Francis**2008**.
[41] H. Zhao, D. Beysens, *Langmuir* **1995**, *11*, 627.
[42] J. Lee, J. Choy, Y. Choi, *Surf. Sci.* **1991**.
[43] H. Merte, C. Yamali, *Wärme - Stoffübertragung* **1983**, *17*, 171.
[44] A.T. Paxson, *Condensation Heat Transfer on Nanoengineered Surfaces*, M.S. Thesis, Massachusetts Institute of Technology, **2011**.

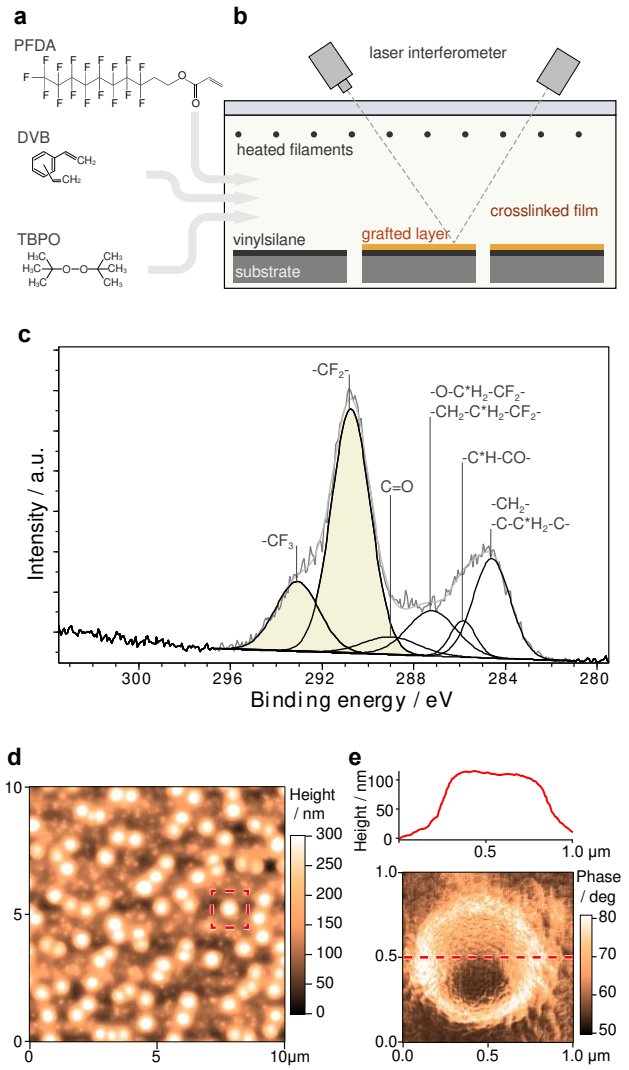

Figure 1. Surface characterization of iCVD p(PFDA-*co*-DVB) coating deposited on a smooth silicon substrate. (**a**) Initiator (TBPO) and reacting species (PFDA and DVB). (**b**) Schematic of deposition chamber and process. (**c**) High resolution angle-resolved XPS spectra taken at 0° takeoff angle. Peaks corresponding to -CF_2- and -CF_3 environments are highlighted. (**d**) 10 x 10 μm AFM height scan of surface topology showing spherulitic texture. Dashed box indicates region of (**e**), 1 x 1 μm AFM phase scan of single roughness feature (bottom) and line height scan (top).

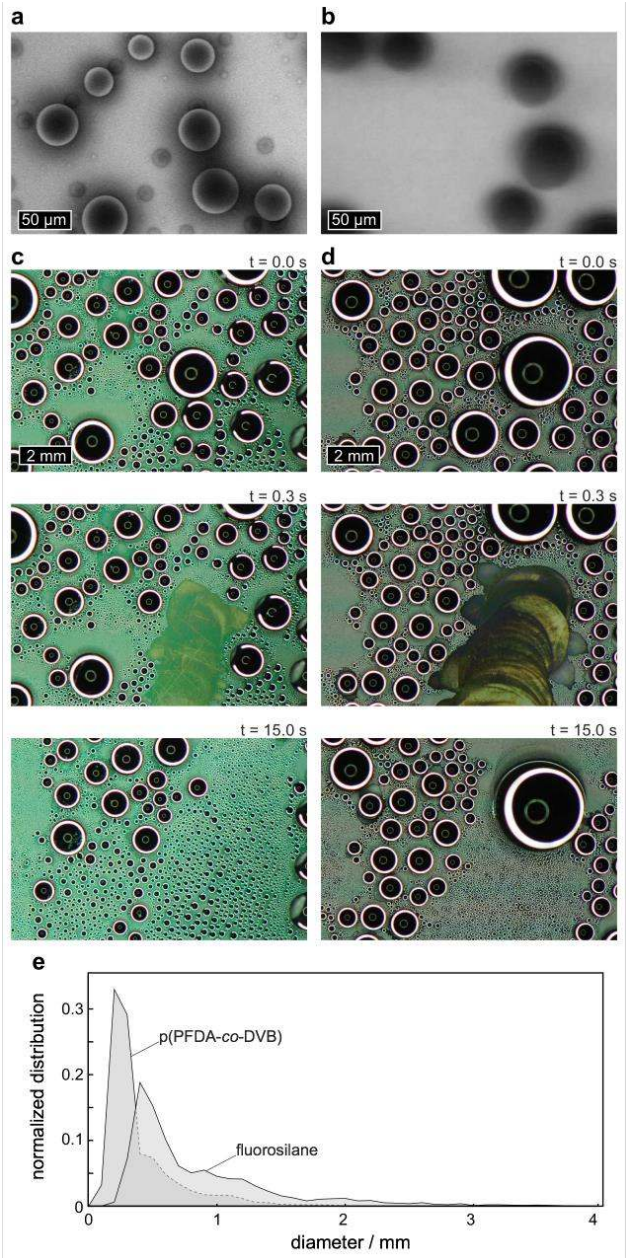

Figure 2. Comparison of water vapor condensation on p(PFDA-*co*-DVB) and fluorosilane coatings deposited on silicon substrates. Environmental scanning electron micrograph of condensation of pure saturated water vapor at 800 Pa and a supersaturation of 1.16 ± 0.05, showing pre-coalescence behavior on (**a**) copolymer and (**b**) fluorosilane surfaces, indicating higher nucleation density on copolymer surface. Photographs of condensation of water vapor in air at 40% R.H. on (**c**) copolymer and (**d**) fluorosilane surfaces immediately before and after a shedding event (top and middle photographs, respectively) and 15 seconds after the shedding event (bottom photograph), indicating smaller departing drop diameter on copolymer surface. (**e**) Time-averaged normalized droplet diameter distributions. Smaller drop sizes on copolymer surface indicate better shedding behavior.

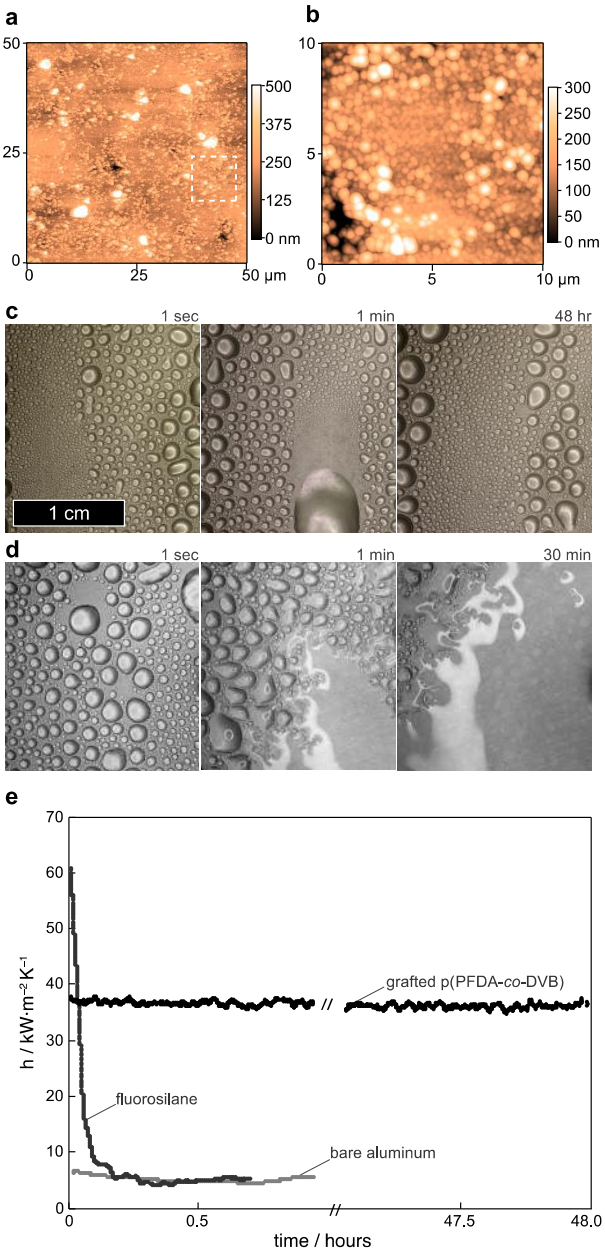

Figure 3. Surface topology and water vapor condensation on p(PFDA-*co*-DVB) coating deposited on an aluminum substrate. (**a**) 50 x 50 µm AFM height scan of surface topology. Dashed box indicates region of (**b**), 10 x 10 µm AFM height scan of surface topology. Photographs during condensation of saturated steam at 100°C and 101 kPa of (**c**) prolonged dropwise condensation on grafted coating over a period of 48 hours and (**d**) degradation of fluorosilane coating over a period of 30 min. (**e**) Heat transfer coefficient of aluminum substrates with no coating, with a fluorosilane coating, and with a grafted p(PFDA-*co*-DVB) coating, plotted vs. time.

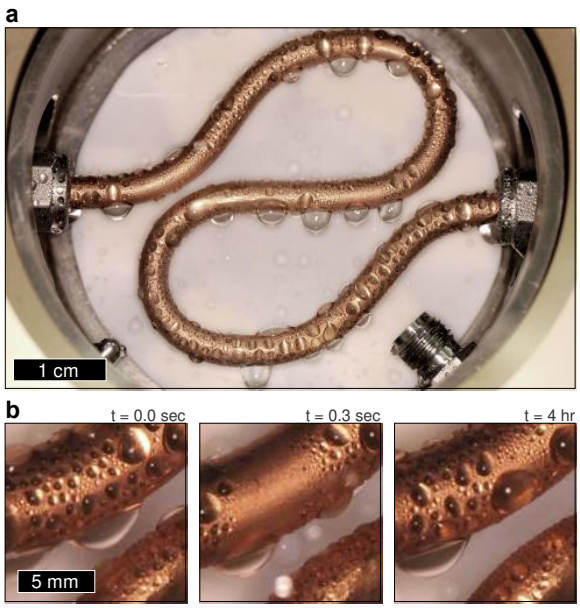

Figure 4. (**a**) Dropwise condensation of saturated steam at 6.9 kPa on a copper tube coated with p(PFDA-*co*-DVB). (**b**) Snapshots immediately before and after a droplet shedding event (left and center photographs, respectively) and 4 hours after shedding event (right photograph).

Table 1. Effect of film thickness on condensation heat transfer coefficient.

thickness [nm]	h [kW m^{-2} K^{-1}]
41.5 ± 2.4	38.1 ± 4.0
59.2 ± 6.6	39.5 ± 4.2